Chalcogenide Letters Vol. 16, No. 11, November 2019, p. 523 - 533

EFFECT OF Fe_2O_3 ON OPTICAL AND STRUCTURAL PROPERTIES OF $80TeO_2$–$(20-x)ZnO$–xFe_2O_3 TELLURITE GLASS SYSTEM

M. F. R. AMIRUDDIN, R. HISAM*, A. K. YAHYA
Faculty of Applied Sciences, Universiti Teknologi MARA, 40450 Shah Alam, Selangor, Malaysia

Ternary $80TeO_2$–$(20-x)ZnO$–xFe_2O_3 glass system was prepared using conventional melt quenching technique to investigate the effect of Fe_2O_3 on structural, thermal and optical properties of the glass system. FTIR analysis shows domination of bridging oxygen (BO) as indicated by intensity of TeO_4 assigned peak (~650cm^{-1}) relative to intensity of TeO_6 assign peak (780cm^{-1}). Shifting of FeO_6 assign peak (~460cm^{-1}) to a higher wavenumber indicates hardening which may be due to increase in rigidity as corroborated by the increase of T_g of the glass system. Direct and indirect optical energy gap, (E^D_{opt} and E^I_{opt}) obtained from UV-Vis spectra analysis showed both values displayed large drop with initial addition of Fe_2O_3 (x=5 mol%) before decreasing at slower rate for x>5 mol%. Both E_{opt} are suggested to decrease with increase of TeO_4 since the energy difference between the highest occupied molecular orbital (HOMO) and lowest unoccupied molecular orbitals (LUMO) of TeO_4 is smaller compared to that of TeO_3.

(Received August 20, 2019; Accepted November 11, 2019)

Keywords: Optical properties, Tellurite glass, HOMO, LUMO

1. Introduction

Tellurium oxide (TeO_2), a well-known oxide based glass are considered as a very promising material due to electrical [1, 2], optical [3-8], magnetic [9] and elastic [10, 11] properties and possesses advantageous properties such as chemical stability, high reflective index and malleability, low phonon energy and high dielectric constant which is good candidate for optical switching and gas sensing material. More interestingly, tellurite glass is non-hygroscopic compare to phosphate glass and borate glass. On the other hand, TeO_2 are known as a conditional glass former which can form a glass network in conjunction with a glass modifier such as WO_3 [12, 13], ZnO [5, 7, 8, 10, 14] iron-oxides [4, 15] or any alkali metal or transition metal oxides. Previously, studies on tellurite glass doped with metal-basis oxides were being widely conducted. Addition of metal oxides in the tellurium glasses shows significant changes not only in physical but also optical properties [5-7, 16, 17].

Study on tellurite glass doped with transition metal oxide shows significant effects on some properties such as structural, electrical, thermal and optical in both binary and ternary glass system [2, 5-8, 11, 16, 18-21]. Previous studies on binary ZnO-TeO_2 [22] or zinc tellurite glass shows that physical properties such as density increase linearly while molar volume decreases with the increment of ZnO content which was suggested to be due to decreases in average interatomic spacing. In addition, optical band gap, E_{opt} decreased while refractive index, n increased suggested due to presence of more non-bridging oxygen (NBO) since NBO has much greater ionic character and lower bond energies. In contrast, studies on temperature dependence of electronic polarizability and optical basicity by V. Dimitrov and T.Komatsu et. al. [23] shows decrease in density with increase in mole fraction of ZnO in xZnO–$(100-x)TeO_2$. Furthermore, at room temperature for x>20 mol% optical properties such as refractive index n, molar polarizability $\alpha_{m,}$ electronic polarizability of oxide ion $\alpha_{o-,}$ and optical basicity Λ decreased. It is suggested that fraction of TeO_3 structural units with NBO content increased as a function of ZnO. Meanwhile, Manning et. al [24] found that refractive indices decrease with the increase of ZnO content and

* Corresponding author: rosdiyana@uitm.edu.my

proposed conversion of TeO_4 units into TeO_3 units reduced polarizability, hence refractive index, n reduced. Coincidently, same behavior on physical and optical properties also found in zinc-tellurite glass by J.G Thorbhan and J.W Zwanziger et. al [25] and Kaur et. al [26]. They suggested that at high concentration of ZnO, networks of ZnO_4 are formed and at low concentration of ZnO acts as network modifier, breaking the Te–O–Te linkages.

On the other hand, several reports on Fe_2O_3 – TeO_2 binary glass system shows an interesting behavior in both physical and chemical properties [27, 28]. Increasing of Fe_2O_3 by concurrent reduction of TeO_2 strongly influenced the magnetic susceptibility but not change the basic TeO_4 trigonal bipyramidal structure units to local TeO_3 indicating the dominance of BO [13]. On the contrary, other study on binary Fe_2O_3–TeO_2 glass system has shown that incorporating Fe_2O_3 in the TeO_2-rich glass network strongly induced depolymerization of TeO_4 units into TeO_{3+1} and TeO_3 units [29] and decreases the density upon adding Fe_2O_3 content.

Previously we reported on the elastic and structural properties of ternary $80TeO_2$–$(20-x)ZnO$–xFe_2O_3 tellurite glass system which shows non-linear increase in elastic constants (longitudinal, C_L, shear, C_s, bulk modulus, K and Young's modulus, E) as well as Debye temperature, θ_D. It was found that both K and E has a large increase at x=0 mol% to x=5 mol% followed by small increase for x>5mol%. Furthermore, Fourier transform infrared (FTIR) studies on $80TeO_2$–$(20-x)ZnO$–xFe_2O_3 glass system reported that formation of BO is more dominant than NBO. In addition, both increment in elastic moduli and θ_D show that additions of Fe_2O_3 strengthen the compound structure by producing more BO as Fe_2O_3 increase. On the other hand, for $20ZnO$-$(80-x)TeO_2$-xFe_2O_3 [30] reported that the glass transition temperature, T_g and thermal stability ΔT increased. It was suggested that the addition of Fe_2O_3 increased the average coordination number and creates strongly bonded network which is also responsible for the increase in thermal stability. Such change brought about by iron on $80TeO_2$–$(20-x)ZnO$–xFe_2O_3 may also influence optical properties of the glass system as reported in other ternary glass such as TeO_2-WO_3-PbO_2 [31, 32], TeO_2-La_2O_3-TiO_2 [33, 34] and WO_3-Ag_2O-TeO_2 [35] glass systems where substitution of transition metal oxides (TMO) influenced the elastic and optical properties of the glass systems. However, for $80TeO_2$–$(20-x)$ ZnO–xFe_2O_3, such study on optical properties has not been carried out.

The aim of this present work is to determine the effect of Fe_2O_3 in $80TeO_2$–$(20-x)$ ZnO–xFe_2O_3 tellurite glass system on its structural and optical properties using FTIR spectroscopy and UV-vis spectroscopy, respectively. Urbach energy (E_U) of the glass system was also calculated in order to elucidate structural disorder of the glass structure. In addition, in order to relate rigidity with the effect of Fe_2O_3 addition, results of DSC study have been presented and discussed.

2. Experiment details

The $80TeO_2$-$(20-x)ZnO$-xFe_2O_3 glass system with x= 0, 5, 10, 15 and 20 mol % were synthesized by melt-quenching technique. The powder of Fe_2O_3 (99.99% purity), ZnO (99.99% purity) and TeO_2 (99.995% purity) were mixed and ground in agate mortar in an hour to reach homogeneity and fined grained mixture. The mixed batches were then melted at 900°C in an hour. The melt was quickly quenched by pouring it on stainless steel plate before annealed at 150°C for 3 hours. The glasses were then grounded into powder to meet the requirement of X-ray diffraction (XRD), IR spectra (FTIR), UV-Vis and differential scanning calorimeter (DSC) measurements. XRD analysis was performed to confirm the amorphous nature of the glass samples by using X'Pert Pro Panalytical diffractometer. The density, ρ of the glass samples were determined using Archimedes principle with xylene as an immersion medium and the relation is:

$$\rho = \left(\frac{W_a}{W_a - W_b}\right)\rho_b \tag{1}$$

where W_a is the glass sample weight in air, W_b is the glass sample weight in xylene and ρ_b is the density of xylene (0.865 g/mL). The corresponding molar volume was calculated using formula:

$$V_m = \frac{M}{\rho} \tag{2}$$

where M is the molar volume and ρ is density.

Infrared (IR) absorption analysis was performed in the region of 400-1000 cm^{-1} with NICOLET 560 spectrometer, using KBr pellets at room temperature. On the other hand, the glass transition temperature, T_g was measured using DSC (NETZSCH DSC 200 F3 model). All samples were heated in porcelain crucible from 100°C to 500°C at the rate of 10°C min^{-1}.

Optical absorption spectra were recorded using Varian Cary 5000 UV-VIS-NIR spectrometer with wavelength range between 200-1000 nm at room temperature. Optical energy band gap for both direct and indirect was obtained from the graph. The optical absorption coefficient α(l) for each photon energy, below and near the edge of each curve is calculated by

$$\alpha(\lambda) = \frac{2.303A}{d} \tag{3}$$

where A is the absorbance and d is thickness of the sample.

The optical absorption coefficient $\alpha(v)$as a function of photon energy hv can be expressed using the Davis and Mott equation that yields the optical energy band gap:

$$\alpha(v) = A\left[(hv - E_{\mathrm{opt}})^p / hv\right] \tag{4}$$

where α is absorption coefficient near the fundamental absorption edge of each spectrum, E_{opt} is optical band gap in eV, A is constant and p is an index which can be assumed to have 1/2, 3/2, 2 or 3, depending on the nature of the electronic transition responsible for absorption. Here p is equal to 1/2 for direct allowed transition, 3/2 for direct forbidden transitions, 2 for indirect allowed transitions and 3 for indirect forbidden transitions. n is determined through a following empirical relation:

$$\frac{n^2 - 1}{n^2 + 2} = 1 - \sqrt{\frac{E_{\mathrm{opt}}}{20}} \tag{5}$$

Relation between molar refraction, refractive index and molar volume is described by the Lorentz-Lorenz equation:

$$R_m = \frac{(n^2-1)}{(n^2+2)} V_m \tag{6}$$

where R_m is molar refraction. The molar refraction is related to structure of the glass and it is proportional to molar electronic polarizability of the material $\alpha(m)$ through the following relation:

$$\alpha(m) = \frac{4}{3\pi N_A} R_m \tag{7}$$

with α_m in ($Å^3$) in Equation (7) can be transformed to the following expression:

$$\alpha(m) = \frac{R_m}{2.52} \tag{8}$$

3. Result and analysis

The XRD pattern for all samples of $80TeO_2$-(20-x)ZnO-xFe_2O_3 (x=0, 5, 10, 15, 20 mol %) glass system confirm the amorphous nature of the glass system (Fig. 1). Table 1 gives the values of density (ρ), and molar volume (V_a). Fig. 2 shows the variation of ρ and V_a with increments of Fe_2O_3 content for $80TeO_2$-(20-x)ZnO-xFe_2O_3 glass system. The figure clearly shows that the value of ρ decreases gradually with addition of Fe_2O_3 content from 6174 kg m^{-1} (x = 0 mol %) to 4638 kg m^{-1} (x = 20 mol %). Meanwhile, as addition of Fe_2O_3 increasing from x = 0 to x = 20 mol%, the

molar volume (V_a) of the glasses also steadily decrease from 2.33x10^{-3} m^3 mol^{-1} to 3.44 x$10^{-3}$$m^3$ mol^{-1}.

Meantime, Fig. 3 shows the FTIR spectroscopy for 80TeO_2-(20-x)ZnO-$x$$Fe_2O_3$ glass system. Four major bands IR absorption bands were observed, namely, 452-456, 578-580, 632-660 and 747-794 cm^{-1}. An abruptly appear peak for x>5mol% at 452-456 cm^{-1} is assign to vibration of FeO_6 octahedral group [36], while 578-580 cm^{-1} peak is assign to stretching vibration of TeO_{3+1} [37]. Meantime, band 632-660 cm^{-1} peak is assign to bending and stretching vibration of TeO_4 trigonal bipyramidal (tbp) group. Wavenumber of 747-794 cm^{-1} is assign to stretching vibration of TeO_3 bipyramidal (bp) unit. Additionally, peak 455 cm^{-1} is assign to vibration of zinc - oxygen bonding respectively [10]. The assignment for the FTIR peak was shown in Table 2. Deconvoluted diagram for x=15mol% using Guassian function (Fig. 4) shows the four-major peak intensity of FeO_6, TeO_{3+1}, TeO_4 and TeO_3 respectively.

The DSC curves for $0 \leq x \leq 20$ mol% of the glass system are shown in Fig. 5. The values of glass transition temperature (T_g), onset crystallization temperature, (T_o), temperature of the first crystallization peak (T_x) and thermal stability, ($\Delta T = T_o - T_g$) are tabulated in Table 3. The replacement of ZnO by Fe_2O_3 leads to an increase of T_g in glass from 317 ˚C (x=0 mol%) to 412˚C (x=20 mol%). The graph of thermal behavior of T_g was illustrated in Fig. 6. Calculated values of ΔT Shows increasing in tempereture at x=0 mol% (67°C) to x=10 mol% (143°C) before slightly decreases at x>10 mol% (143°C - 129°C) respectively.

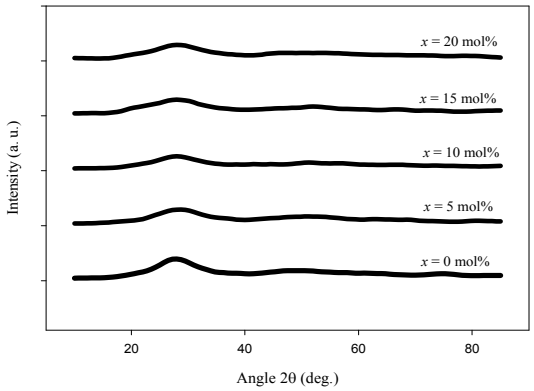

Fig. 1. XRD pattern of 80TeO_2-(20-x)ZnO-xFe_2O_3 (x=0, 5, 10, 15, 20 mol %) glass system.

Table 1. Density, ρ and molar volume, V_a of 80TeO_2-(20-x)ZnO-xFe_2O_3 (x=0, 5, 10, 15, 20 mol%) glass system.

x (mol%)	**ρ (± 20 kg/m^3)**	**V_a (± 0.003 m^3/mol) x 10^{-5}**
0	6174	2.33
5	5715	2.58
10	4955	3.06
15	4702	3.31
20	4638	3.44

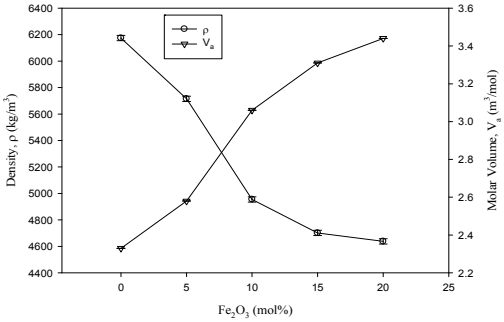

Fig. 2. Density, ρ and molar volume, V_a of $80TeO_2$-(20-x)ZnO-xFe_2O_3 (x=0, 5, 10, 15, 20 mol %) glass system.

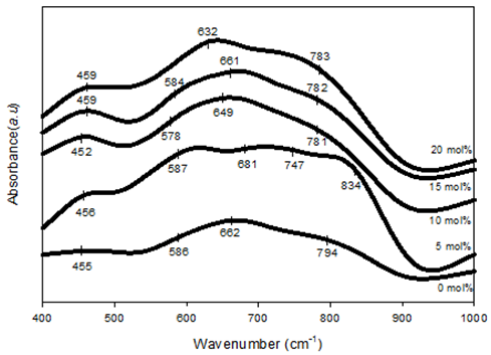

Fig. 3. The FTIR spectroscopy of $80TeO_2$-(20-x)ZnO-xFe_2O_3 (x=0, 5, 10, 15, 20 mol %) glass system.

Table 2. Wavenumber and their assignments for IR spectra for $80TeO_2$-(20-x)ZnO-xFe_2O_3 (x=0, 5, 10, 15, 20 mol%) glass samples.

Wavenumber (cm^{-1})	Assignments
~452-456	Vibration of FeO_6 octahedral group
~578-587	Stretching vibration of TeO_{3+1}
~632-681	Bending and stretching vibration of TeO_4 trigonal bipyramidal (tbp) group
~747-794	Stretching vibration of TeO_3 bipyramidal (bp) unit.

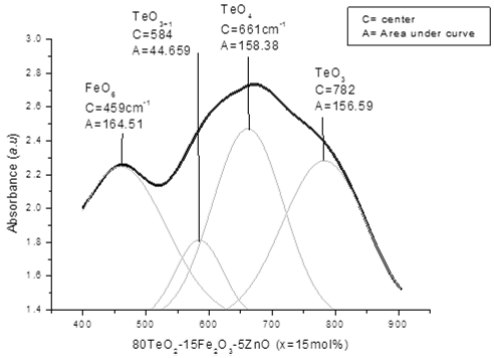

Fig. 4. Deconvoluted IR spectra of the $80TeO_2$-$15Fe_2O_3$-5ZnO glass sample using a Gaussian type function.

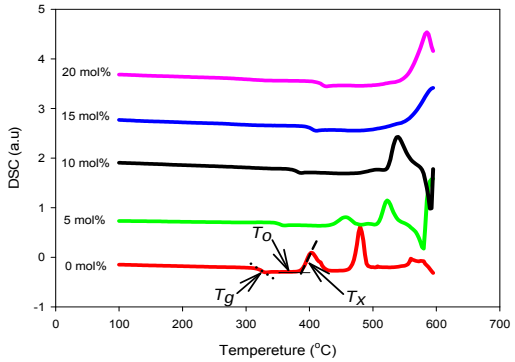

Fig. 5. DSC curves of $80TeO_2$-(20-x)ZnO-xFe_2O_3 (x=0, 5, 10, 15, 20 mol %) glass system.

Table 3. Values of temperature glass transition temperature (T_g), onset crystallization temperature, (T_o), temperature of the first crystallization peak (T_x) and thermal stability, (ΔT) of $80TeO_2$-(20-x)ZnO-xFe_2O_3 (x=0, 5, 10, 15, 20 mol %) glass system.

***x* (mol%)**	**T_g (°C)**	**T_o (°C)**	**T_x (°C)**	**$\Delta T = T_o - T_g$ (°C)**
0	317	384	403	67
5	348	433	457	85
10	374	517	539	143
15	393	527	596	134
20	412	541	585	129

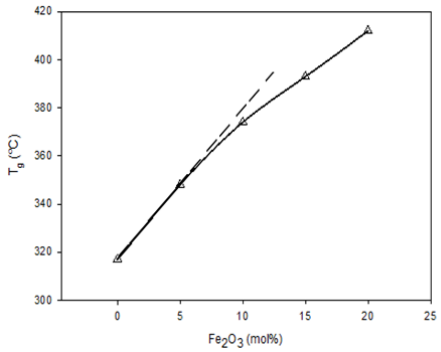

Fig. 6. Graph of T_g behavior of $80TeO_2$-(20-x)ZnO-xFe_2O_3 (x=0, 5, 10, 15, 20 mol %) glass system.

The absorption spectra taken at room temperature for all glass system are shown in Fig. 7. The absorption edges are shifting as addition iron content increases. The calculated values of optical energy gap (E_{opt}) for direct (E^D_{opt}) and indirect (E^I_{opt}), Urbach energy (E_u), refractive index (n), molar fraction (R_m) and electronic polarizability, (α_m) was tabulated in Table 4.

Optical energy gap was determined from Eq. (4) by extrapolating the α to zero absorption in the $(\alpha hv)^{1/2}$ vs hv for E^I_{opt} and $(\alpha hv)^{3/2}$vs hv for $E^D_{opt.}$ as shown in Fig. 8 and Fig. 9 respectively. The comparison graph of calculated value between those two are shown in Fig. 10. Both the gaps for the glass systems shows a large drop from x=0 mol% to x=5 mol% before slightly decreases at x>5 mol%.

Refractive index, n is one of important properties of optical glass and can be obtained using Eq. (5). The calculated n shows an opposite trend to E^D_{opt} (Fig. 11) where it was initially increase from 2.62 (x=0 mol%) to 3.05 (x=5 mol%) followed by slightly increase to 3.53 at x=20

mol%. On the other hand, molar fraction, R_m can be described by Lorentz-Lorentz equation (Eq.6). The equation gave the average molar refraction for isotropic substance, which co-relate with structure of the glass by V_m and it is proportional to molar electronic polarizability, α_m (Eq. 7 and Eq. 8). The α_m was gradually increase from 6.12Å^3 at x= 0 mol% to 10.83Å^3 at x= 20 mol% (Fig. 13). Meantime, the E_u can be obtained by extrapolating the graph lnα vs $h\upsilon$ as shown in Fig. 12. The Urbach energy, E_u has the lowest value at x=0 mol% (0.26eV). The values tend to increase as Fe_2O_3 content increased as shown in Fig. 13 above.

Table 4. Direct optical energy band gap, E^D_{opt}, Indirect optical energy band gap, E^I_{opt} Urbach energy, E_u, Refractive index, n, Molar fraction, R_m and Electronic polarizability, α_m of $80TeO_2$-(20-x)ZnO-xFe_2O_3 (x=0, 5, 10, 15, 20 mol %) glass system.

x	E^I_{opt} (eV)	E^D_{opt} (eV)	E_u (eV)	N	R_m ($cm^3\ mol^{-1}$)	α_m (Å^3)
0	2.29	3.41	0.27	2.62	15.43	6.12
5	1.41	2.38	0.75	3.05	18.93	7.51
10	1.32	2.26	0.81	3.11	22.77	9.04
15	1.04	2.14	0.99	3.34	25.58	10.15
20	0.86	2.00	1.23	3.53	27.29	10.83

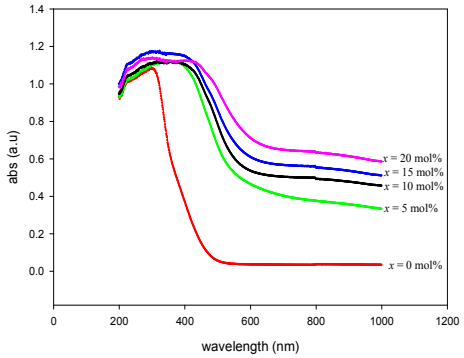

Fig. 7. Optical absorption spectra taking at room temperature of $80TeO_2$-(20-x)ZnO-xFe_2O_3 (x=0, 5, 10, 15, 20 mol %) glass system.

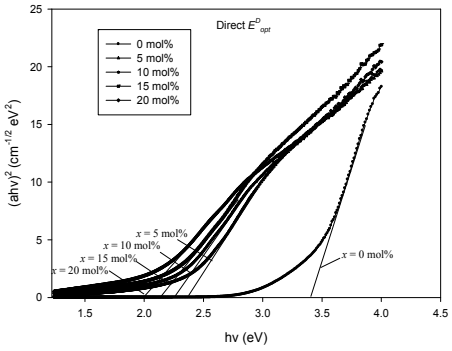

Fig. 8. Plot of $(\alpha h\upsilon)^2$ as a function of $h\upsilon$ for $80TeO_2$-(20-x)ZnO-xFe_2O_3 (x=0, 5, 10, 15, 20 mol %) glass system.

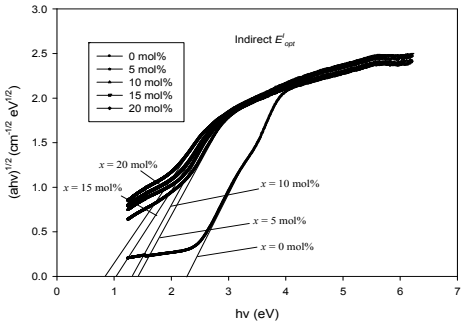

Fig. 9. Plot of $(\alpha h\nu)^{1/2}$ as a function of hν for $80TeO_2$-(20-x)ZnO-xFe_2O_3 (x=0, 5, 10, 15, 20 mol %) glass system.

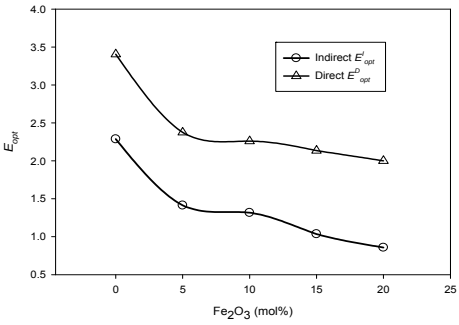

Fig. 10. Direct optical energy band gap, E^D_{opt} and indirect optical energy band gap, E^I_{opt} of $80TeO_2$-(20-x)ZnO-xFe_2O_3 (x=0, 5, 10, 15, 20 mol %) glass system.

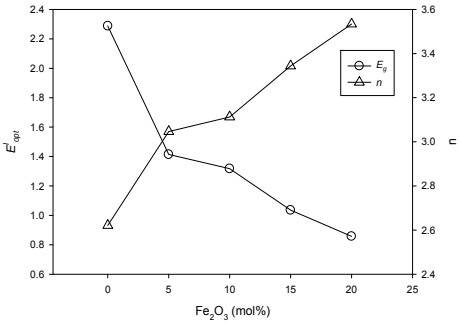

Fig. 11. Indirect optical energy band gap, E^I_{opt} and refractive index, n of $80TeO_2$-(20-x)ZnO-xFe_2O_3 (x=0, 5, 10, 15, 20 mol %) glass system.

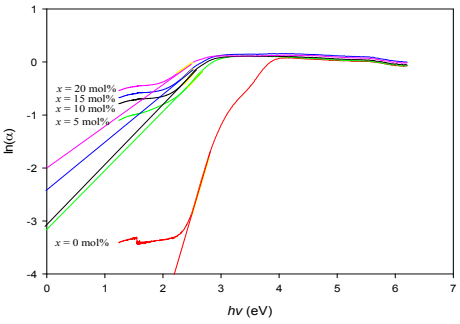

Fig. 12. Determining Urbach energy, E_u of $80TeO_2$-(20-x)ZnO-xFe_2O_3 (x=0, 5, 10, 15, 20 mol %) glass system.

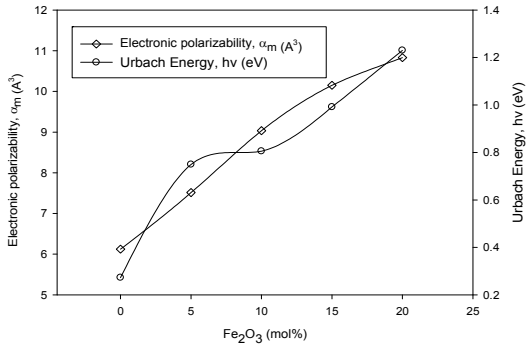

Fig. 13. Urbach energy, E_u and electronic polarizability, α_m of $80TeO_2$-(20-x)ZnO-xFe_2O_3 (x=0, 5, 10, 15, 20 mol %) glass system.

4. Discussions

Density analysis is one of the important physical studies to indicate the structural compactness of a glass system. In our present study, increasing Fe_2O_3 content results in decreasing of ρ while V_m increased. The behavior of ρ can be due to either change in molar mass (M_a) or molar volume V_a but the substitution of heavier Fe_2O_3 (molecular mass 159.69 g/mol) compared to lighter ZnO (molecular mass 81.408 g/mol) caused density to decrease suggesting that the increase in V_a is larger in comparison to the increase in M_a [10]. It is also suggested that shorter Zn – O bonds were replaced by longer Fe – O bonds, leading to formation of more open network structure [32]. The glass transition temperature (T_g) is well known to be a structural parameter depending on the bond strength, degree of cross-link density and closeness of packing [43]. The increase in T_g (Fig. 6) could be caused by the replacement of ZnO by Fe_2O_3 which has greater bond strength (409 kJmol^{-1}) than ZnO (151 kJmol^{-1}) [43, 44]. Moreover, the increase in the value of T_g can be corroborated to support the increase in rigidity of the glass system.

Our result on increase in rigidity due to increase of Fe_2O_3 was evidenced by FTIR analysis where it was observed that FeO_6 assigned peak was shifted to higher wavenumbers. Meantime, peak intensity of TeO_4 *tbp* at 661cm^{-1} (x=15mol%) which was higher compared to peak intensity of TeO_3 *tp* at 782cm^{-1} indicates the ascendancy of BO as shown in the deconvoluted diagram (Fig. 4). In addition, the shifting of TeO_4 assigned peak as well as the increase its intensity at around 631-681cm^{-1} for x=0mol% to x=20mol% samples indicates the formation of BO. Meanwhile, formation of NBO was indicated by TeO_3 *tp* assigned shoulder at around 780cm^{-1}. The presence of both BOs and NBOs indicates some form of competition may be present between them. However, in our studies, the intensity of TeO_4 assigned peak was more abundant which indicates the dominance of BO compared to NBO on the glass system. Our suggestion of more dominant BO was supported by the increase in rigidity from the DSC studies and the result in rigidity was collaborated by increase in elastic modulus studies reported by Azianty et. al [10].

Optical absorption of photon in the glasses can take place by direct or indirect transition. Many studies reported that the indirect transition which involves both photon and phonon are more prominent in amorphous materials [12, 13, 39]. However, here, for a comparison, both direct and indirect transitions were taken into consideration in order to determine the most suitable transition for this glass system. Generally in oxide glasses, increasing BO usually leads to increasing E_{opt} as electrons are bound more tightly for BO and are harder to excite compared to NBO [23, 40]. However, for this glass system, we observed that E_{opt} for x=0-20 mol % (Fig. 10) decreased as BO content increased as shown in FTIR analysis. Such behavior could be understood by considering previous report on ab-initio molecular orbital calculation results which showed that the energy difference of the highest occupied molecular orbital (HOMO) and lowest unoccupied molecular orbital (LUMO) state of TeO_4 is smaller than those of TeO_3 [41].

The increase in n (Table 4) is essentially a consequent of the decrease in E_{opt} as calculated using Eq.5. The increase could also be understood due to the increase in total electronic

polarizability as shown in Fig. 13 since Fe_2O_3 has larger electronic polarizability (2.647Å^3) compared to ZnO (2.612Å^3). Our result of the increase in *n* with the increase in BO is not unique to the present glass system but has also been reported for several glass systems such as TeO_2–Nb_2O_5–ZnO[8] and TeO_2–Nb_2O_5–ZnO–PbO [42] glass systems. On the other hand, the increasing behavior of Urbach energy (Fig. 13) indicates the increase in defect of the glass network. In glass, the presence of defect has been suggested to be closely related to the amount of NBO [3, 4, 13].

5. Conclusions

Fe_2O_3 substitution in $80TeO_2$-(20-x)Fe_2O_3–xZnO glass system has caused larger number of TeO_4 tbp over TeO_3 tbp which indicate the dominance of BO on the glass system as indicated by FTIR analysis. Optical band gap shows a decreasing behaviour and was suggested be due to smaller energy difference between the highest occupied molecular orbital (HOMO) and lowest unoccupied molecular orbitals (LUMO) of TeO_4 compared to that of TeO_3. Refractive index, *n* calculated from E_{opt} values shows an increase with Fe_2O_3 which may be due to the increase in electronic polarizability. Urbach energy, E_u increased suggesting that defects in the glass system increased with increasing Fe_2O_3.

Acknowledgements

The authors express gratitude to the Institute of Research Management and Innovation (IRMI) and Universiti Teknologi MARA, Selangor, Shah Alam, Malaysia for funding this research under the BESTARI Grant (600-IRMI/DANA 5/3/BESTARI (130/2018)).

References

[1] M. R. Tripathy, Materials Letters **61**(2), 585 (2007).
[2] H. Satou, H. Sakata, Materials Chemistry and Physics **65**(2), 186 (2000).
[3] W. Widanarto, M. R. Sahar, S. K. Goshal, R. Ariffin, M. S. Rohani, K. Hamzah, Journal of Magnetism and Magnetic Materials **326**, 123 (2013).
[4] W. Widanarto, M. R.Sahar, S. K. Goshal, R. Ariffin, M. S. Rohani, K. Hamzah, M. Jandra, Materials Chemistry and Physics **138**(1), 174 (2013).
[5] F. Vetrone, J. C. Boyer, J. A. Capobianco, A. Speghini, M. Bettinelli, Applied Physics Letters **80**(10), 1752 (2002).
[6] H. Xia, Q. Nie, J. Zhang, J. Wang, Materials Letters **57**(24-25), 3895 (2003).
[7] J. Li, Z. Sun, X. Zhu, H. Zeng, Z. Xu, Z. Wang, J. Lin, W. Huang, R.S. Armstrong, P. A. Lay, Optical Materials **25**(4), 401 (2004).
[8] J. Lin, W. Huang, Z. Sun, C. S. Ray, D. E. Day, Journal of Non-Crystalline Solids **336**(3), 189 2004).
[9] K. Tanaka, H. Akamatsu, S. Nakashima, K.Fujita, Journal of Non-Crystalline Solids **354**(12-13), 1347 (2008).
[10] S. Azianty, A. K. Yahya, M. K. Halimah, Journal of Non-Crystalline Solids **358**(12-13), 1562 (2012).
[11] H. Afifi, S. Marzouk, Materials Chemistry and Physics **80**(2), 517 (2003).
[12] G. Upender, C. S. Devi, V. C. Mouli, Materials Research Bulletin **47**(11), 3764 (2012).
[13] G. Upender, S. Ramesh, M. Prasad, V. G. Sathe, V. C. Mouli, Journal of Alloys and Compounds **504**(2), 468 (2010).
[14] D. Linda, J. R. Duclére, T. Hayakawa, M. Dutreilh-Colas, T. Cardinal, A. Mirgorodsky, A. Kabadou, P. Thomas, Journal of Alloys and Compounds **561**, 151 (2013).
[15] S. Annamalai, R. P. Bhatta, I. L. Pegg, B. Dutta, Journal of Non-Crystalline Solids **358**(11), 1380 (2012).
[16] M. M. El-Desoky, Journal of Non-Crystalline Solids **351**(37-39), 3139 (2005).

[17] R. Kumar Singh, A. Srinivasan, Journal of Magnetism and Magnetic Materials **322**(14), 2018 (2010).
[18] A. Meeder, D. F. Marrón, A. Rumberg, M. C. Lux-Steiner, V. Chu, J. P. Conde, Journal of Applied Physics **92**(6), 3016 (2002).
[19] O. Noguera, T. Merle-Méjean, A. P. Mirgorodsky, M. B.Smirnov, P. Thomas, J. C. Champarnaud-Mesjard, Journal of Non-Crystalline Solids **330**(1-3), 50 (2003).
[20] Y. B. Saddeek, L. A. El Latif, Physica B: Condensed Matter **348**(1-4), 475 (2004).
[21] V. V. Gowda, R. V. Anavekar, K. J. Rao, Journal of Non-Crystalline Solids **351**(43-45), 3421 (2005).
[22] H. A. A. Sidek, S. Rosmawati, Z. A. Talib, M. K. Halimah, W. M. Daud, American Journal of Applied Sciences **6**(8), 1489 (2009).
[23] T. Komatsu, N. Ito, T. Honma, V. Dimitrov, Solid State Sciences **14**(10), 1419 (2012).
[24] S. Manning, H. Ebendorff-Heidepriem, T. M. Monro, Optical Material Express **2**(2), 140 (2012).
[25] J. G. Thorbahn, J. W. Zwanziger, Journal of Non-Crystalline Solids **381**, 48 (2013).
[26] A. Kaur, A. Khanna, C. Pesquera, F. González, V. Sathe, Journal of Non-Crystalline Solids **356**(18-19), 864 (2010).
[27] L. Murawski, R.J. Barczyński, Solid State Ionics **176**(25-28), 2145 (2005).
[28] A. Mekki, G. D. Khattak, L. E. Wenger, Journal of Non-Crystalline Solids **352**(30-31), 3326 (2006).
[29] N. A. Zarifah, M. K. Halimah, M. Hashim, B. Z. Azmi, W. M. Daud, Chalcogenide Letters **7**(9), 565 (2010).
[30] P. S. Rani, R. Singh, Journal of Physics and Chemistry of Solids **74**(2), 338 (2013).
[31] G. Upender, V. C. Mouli, Journal of Molecular Structure **1006**(1-3), 159 (2011).
[32] S. Azianty, A. K. Yahya, Journal of Non-Crystalline Solids **378**, 234 (2013).
[33] I. N. Sapian, M. I. M. Yusof, A. K. Yahya, Chalcogenide Letters **11**(10), 471 (2014).
[34] W. Stambouli, H. Elhouichet, M. Ferid, Journal of Molecular Structure, **1028**, 39 (2012).
[35] M. M. Umair, A. K. Yahya, M. K. Halimah, H. A. A. Sidek, Journal of Materials Science & Technology **31**(1), 83 (2015).
[36] N. Baizura, A. K. Yahya, Journal of Non-Crystalline Solids **357**(5), 2810 (2011).
[37] S. Rada, M. Neumann, E. Culea, Solid State Ionics **181**(25-26), 1164 (2010).
[38] S. Laila, S.N. Supardan, A.K. Yahya, Journal of Non-Crystalline Solids **367**, 14 (2013).
[39] M. M. Umair, A. K. Yahya, Materials Chemistry and Physics **142**(2-3), 549 (2013).
[40] G. Upender, V. G. Sathe, V. C. Mouli, Physica B: Condensed Matter, **405**(5), 1269 (2010).
[41] B. Jeansannetas, S. Blanchandin, P. Thomas, P. Marchet, J. C. Champarnaud-Mesjard, T. Merle-MeHjean, B. Frit, Journal of Solid State Chemistry **146**, 329-335 (1999).
[42] A. E. Al-Salami, M. Hotzel, Bulletin of Materials Science **35**(6), 961 (2012).
[43] H. Es-Soufi, L. Bih, B. Manoun, P. Lazor, Non-Crystalline Solids, **463**, 12 (2017).
[44] R. Hisam, A. K. Yahya, Chalcogenide Letters, **13**(4), 145 (2016).